RSC Advances

ROYAL SOCIETY OF CHEMISTRY

www.rsc.org/advances

RSC Advances

ARTICLE

A NIR-to-NIR upconversion luminescence system for security printing applications

Received 00th January 20xx,
Accepted 00th January 20xx

DOI: 10.1039/x0xx00000x

www.rsc.org/

A. Baride,[a] J. M. Meruga,[b] C. Douma,[a] D. Langerman,[c] G. Crawford,[b] J. J. Kellar,[b] W. M. Cross[b] and P. S. May*[a]

A covert print-and-read system is demonstrated based on NIR-to-NIR upconversion luminescence. Inks activated with Yb^{3+}/Tm^{3+} doped β-$NaYF_4$ upconversion nanoparticles were used to print covert features on various substrates, including paper, epoxy resin, and circuit boards. The Yb^{3+}/Tm^{3+} doping concentrations were optimized to maximize the brightness of 800 nm upconversion emission excited with 980 nm light, while simultaneously minimizing unwanted blue upconversion. Images printed with the NIR-optimized inks are invisible to the naked eye under ambient lighting or under 980-nm excitation. NIR-to-NIR images are easily captured, however, using an inexpensive, modified point-and-shoot CCD camera, even at modest excitation power densities (1.5 W/cm^2). It is demonstrated that the latent images can also be read through select hard or soft coatings which are opaque to visible light, such as black inkjet print, or dyed epoxy resin, without significant attenuation of brightness. The ability to protect the printed images with durable, opaque coatings increases the tamper-resistance and the covertness of the system; removes the requirement that the print be invisible on the bare substrate; and blocks any visible emission that might be present, even under very high excitation power densities.

Introduction

Counterfeiting is a major concern for corporate, federal and state organizations. Counterfeits compromise the security, identity and value of products, documents, IDs and currency, thereby exerting a strong negative impact on societal financial and social wellbeing. Counterfeiting of integrated circuits (ICs) is a major concern, because of its potential to compromise the performance of a wide range of critical infrastructure, ranging from healthcare devices to military equipment to space hardware.[1, 2] Counterfeit ICs are often fraudulent or degraded products that have been either rejected during quality control or recycled from waste. An effective supply-chain management program, supported by strong track-and-trace security features, is an effective deterrence to counterfeiting.[1] A strong security feature embeds information in the product and resists tampering, duplication or destruction without damaging product integrity. In this study, we describe a print-and-read system for security applications based on NIR-to-NIR upconversion inks, in which the security feature is covert, and can be protected from tampering by hard opaque coatings.

Upconversion phosphors emit at wavelengths shorter than that of the excitation light. Lanthanide-ion-doped β-$NaYF_4$ is recognized for exceptionally efficient near infrared (NIR)-to-visible upconversion upon excitation with 980 nm light.[3-7] The concentrations and combinations of lanthanide dopants influence both the wavelength and the intensity of the upconversion emission. Applications of upconversion nanomaterials include sensors,[8-12] bio-imaging,[13-17] drug delivery[18, 19] and security / anti-counterfeiting.[20-29] Our group has conducted seminal work in using upconversion inks for security printing, including the demonstration of 'invisible QR codes' for security printing and anti-counterfeiting applications.[20-22] The inks are a formulation of upconversion nanoparticles (UCNPs) dispersed in a polymer base. When used to print text or features (e.g. QR codes) on paper, the upconversion ink is invisible to the eye under ambient conditions or UV excitation, but becomes visible upon excitation with 980 nm light.[21] We have recently reported an RGB system for full-color printing using primary color red, green and blue upconversion activated with 10%Er^{3+}/2%Tm^{3+},

[a] Department of Chemistry, University of South Dakota, 414 E Clark St., Vermillion, SD 57069 E-mail: Stanley.May@usd.edu.

[b] Materials and Metallurgical Engineering, [c] Electrical and Computer Engineering, South Dakota School of Mines and Technology, 501 E Saint Joseph St., Rapid City, SD 57701.

Electronic Supplementary Information (ESI) available: [details of any supplementary information available should be included here]. See DOI: 10.1039/x0xx00000x

17%Yb^{3+}/3%Er^{3+} and 25%Yb^{3+}/0.3%Tm^{3+} nanoparticles, respectively.[20]

Co-doping solid-state systems using Tm^{3+} as an activator and Yb^{3+} as a sensitizer is a common strategy for producing NIR-to-blue upconversion phosphors.[20, 21, 30-36] β-$NaYF_4$ UCNPs doped with Yb^{3+} and Tm^{3+} are well known for NIR-to-blue upconversion emission (440-500 nm).[20, 21, 30, 31] These 'blue' UCNPs, however, also emit 800 nm NIR light, which is invisible to the naked eye, but is also much more intense than the visible blue emission.[21] Doping composition has a significant effect on the absolute and relative quantum efficiency of various emission bands. The 25%Yb^{3+}/0.3%Tm^{3+} doping combination is optimized for blue upconversion emission.[37] Zhang *et al.* studied the effect of Tm^{3+} concentration on blue and NIR upconversion efficiency in 18 nm 20%Yb^{3+}/(0.3-4%Tm^{3+}) doped β-$NaYF_4$ nanoparticles.[38] The group reported that the blue emission is quenched as the Tm concentration increases, but no significant change was observed in 800 nm emission over this doping range. In contrast, Wang *et al.* reported an increase in 800 nm emission with increasing Tm concentration from 0.2% to 2% Tm^{3+} in α-$NaYF_4$ UCNPs co-doped with 20%Yb^{3+}.[39] To date, however, the optimum doping combination for achieving maximally bright and spectrally pure 800 nm emission has not been reported for β-$NaYF_4$ UCNPs. For our purposes, maximizing the absolute per-particle brightness at 800 nm is of paramount importance.

In this study, we compare the 980-to-800 nm upconversion efficiency for four doping compositions, 25%Yb^{3+}/0.3%Tm^{3+} (optimized for blue), 25%Yb^{3+}/2%Tm^{3+}, 48%Yb^{3+}/2%Tm^{3+} and 46%Yb^{3+}/4%Tm^{3+} and evaluate the optimum doping for the 800 nm NIR emission. Further, we explore the security printing applications of NIR-to-NIR upconversion emission from Yb^{3+}/Tm^{3+} doped UCNPs and strategies for tamper-resistant security applications of these materials. NIR-to-NIR upconversion is very advantageous for anti-counterfeiting, because most common organic materials are transparent to the 980 nm excitation and 800 nm emission. Consequently, printed features can be excited and read through hard polymer or epoxy coatings. Moreover, these coatings can be completely opaque to visible light, as long as the transmittance is high at 800 nm and 980 nm. A system of markings coated with an opaque epoxy layer would be difficult to detect and quite tamper resistant. In this study, we also demonstrate the excitation and capture of NIR-to-NIR images of UCNPs coated with NIR transparent materials that are either transparent or opaque in the visible range. The NIR luminescent images store information that is not visible to the naked eye, but can be captured with an inexpensive CCD camera.

In addition to the security printing applications discussed here, NIR-to-NIR UCNPs show promise for use in bio-imaging,[40-43] because both the excitation (980 nm) and emission (800 nm) wavelengths fall within the biological transparency window.[42] Therefore, 800 nm emission from UCNPs loaded into biological tissue can be imaged by exciting with 980 nm light.

We propose four scenarios for the use of NIR-to-NIR upconversion inks for security printing, as illustrated in Figure 1: A) covert codes printed on a substrate; B) covert codes embedded within a polymer; C) covert codes printed on a hard substrate and subsequently coated with a transparent polymer; and D) covert codes printed on a hard substrate and subsequently coated with an polymer that is opaque to visible light.

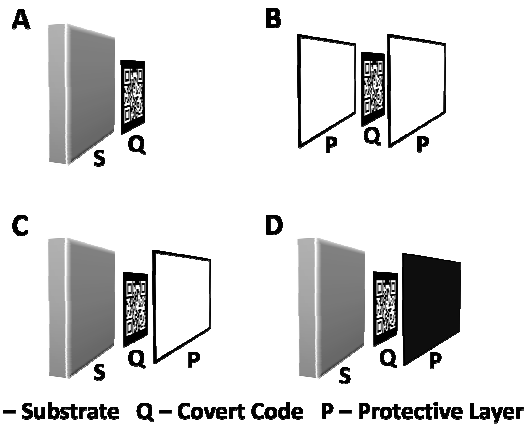

Figure 1: Four scenarios for application of NIR-to-NIR upconversion inks in security printing. A) covert code printed on an opaque substrate. B) covert code laminated between transparent laminates. C) covert code on a substrate protected by a transparent laminate. D) covert code on a substrate protected by an opaque laminate.

Protected codes or symbols encoding critical product information are ideally suited for safeguarding integrated circuits (ICs) and electronic circuit boards from counterfeiting threats. Tampering with markings integrated within the IC packaging without damaging the component would be a difficult task. Integrated circuits are often enclosed in an epoxy case (or mold compound) and electronic circuit boards are frequently coated with polymer films. We choose an epoxy polymer as the protecting layer in our experiments. Epoxy is chemical resistant and insoluble in common solvents, making it difficult to remove in order to reach the embedded code. Moreover, it is highly transmissive in the NIR region. We use electronic circuit boards as an example substrate to demonstrate the potential application of NIR-to-NIR upconversion in security printing and anti-counterfeiting.

Experimental Section

Materials: Yttrium oxide (99.99%), ytterbium oxide(99.9%), thulium oxide(99.9%) and oleic acid (90%) were obtained from Alfa Aesar; 1-octadecene (90%) from Aldrich; methyl benzoate (99%), sodium acetate trihydrate (99%) from Acro Organics; sodium fluoride (99%) from Fisher Scientific; acetic acid (glacial, 99.9%) from Pharm Co.; poly(methyl methacrylate) beads (M.W. 15,000) from Scientific Polymer Products. Black thermo-bubble- jet ink was purchased from Hobbicolors (DJC-

45060-0-A). Ready-to-mix epoxy resins were purchased from commercial retailers.

Synthesis of UCNPs: The UCNPs synthesis procedure is similar to the procedure reported by Lin *et al.* with a few modifications.[44] Yttrium oleate ($Y(OA)_3$), ytterbium oleate ($Yb(OA)_3$) and thulium oleate ($Tm(OA)_3$) precursor solutions, 25 mL each, were prepared as described by Lin *et al.*[44] The resulting $Y(OA)_3$, $Yb(OA)_3$, and $Tm(OA)_3$ solutions have concentrations of 0.2 mmol/mL of Y^{3+}, 0.1 mmol/mL of Yb^{3+}, and 0.01 mmol/mL of Tm^{3+}, respectively.

To prepare UCNPs, $CH_3COONa{\cdot}3H_2O$ (2 mmol), NaF (4 mmol), 1-ODE (16 mL) and appropriate amounts of $Y(OA)_3$, $Yt(OA)_3$, and $Tm(OA)_3$ precursor solutions were combined in a 50 mL flask. The composition of the precursor solution determines the doping concentration of Yb^{3+}/Tm^{3+}. For 25%Yb^{3+}/0.3%Tm^{3+}: 3.74 mL $Y(OA)_3$, 2.5 mL $Yt(OA)_3$ and 0.3 mL $Tm(OA)_3$; for 25%Yb^{3+}/2%Tm^{3+}: 3.65 mL $Y(OA)_3$, 2.5 mL $Yt(OA)_3$ and 2 mL $Tm(OA)_3$; for 48%Yb^{3+}/2%Tm^{3+}: 2.5 mL $Y(OA)_3$, 4.8 mL $Yt(OA)_3$ and 2 mL $Tm(OA)_3$; and for 46%Yb^{3+}/4%Tm^{3+}: 2.5 mL $Y(OA)_3$, 4.6 mL $Yt(OA)_3$ and 4 mL $Tm(OA)_3$ were added. Additional oleic acid was added to bring the total volume of the reaction mixture to 32 mL. The reaction mixture was heated under vacuum at 100 °C for 1 hour to remove volatile solvents and then the vacuum was replaced with a gentle stream of Ar gas. The temperature was increased to 320 °C and reaction was continued for another 2.5 hours. The UCNP product was washed three times by precipitation with acetone re-dispersing in toluene and precipitating with acetone. The UCNPs were dried under vacuum at 65 °C for 24 hours. The size and morphology of the UCNPs was characterized by TEM (FEI Tecnai, 120 kV). (See Supporting Information, Figure S1). The UCNP exhibit a hexagonal morphology with an average size of 112 ± 12 nm. The product UCNPs are phase pure β-$NaYF_4$ nanocrystals (See Supporting Information, Figure S2) as determined by PXRD.

Spectroscopy: Steady-state spectroscopy was performed by exciting 1 wt% dispersions of UCNPs in toluene with a 980 nm CW laser (MDL-N-980, Opto Engine LLC) with power densities between 5 - 35 W/cm^2. Emission spectra were recorded with a miniature spectrophotometer (BLUE-Wave, StellarNet). An 850 nm short-pass filter (4 OD, Edmund, #64-334), was used to block the excitation light from the spectrophotometer. Emission spectra were corrected for the instrument response to give relative photon flux per wavelength interval.

Epoxy film preparation: Epoxy films of desired thickness were prepared from ready-to-mix epoxy resins. A commercially available epoxy (*Loctite Quick Set Epoxy*) was used to prepare epoxy films. The epoxy comes in a two- syringe dispenser with epoxy resin in one syringe and hardener in other syringe. A thin coat of epoxy was prepared by mixing the hardener and the epoxy resin and coating the epoxy mixture on a substrate using a glass slide as an applicator. The black epoxy was prepared by mixing 0.06 mL of black inkjet ink (Hobbicolors) to approximately 2 mL of epoxy mixture. Epoxy thin film was prepared by applying a smear of epoxy mixture on a polypropylene sheet and the film was carefully peeled-off after drying.

Preparation of Inks and Printing: The upconversion inks were prepared as described by Blumenthanl et al.[22] In brief, 5 wt% of UCNPs were dispersed in a solution of 1 wt% of PMMA in a mixture toluene/methyl benzoate (9:1). The inks were printed on plain paper, an electronic circuit board, and an epoxy film using an Optomec aerosol-jet printer.

NIR Imaging: NIR imaging was performed with a point-shoot camera modified to detect NIR signal. The NIR filter in front of the CCD chip was carefully removed from a Canon A470 point-and-shoot camera to capture NIR images. Unless specified, all images were captured using a 1 second exposure, ISO 400, f/5.8 exciting with 980 nm CW laser (1.5 W/cm^2) in ambient lighting from a low-wattage lamp. An 850 nm short-pass filter was used to block excitation light from entering into the camera.

Results and Discussion

Optimization of doping composition for NIR-to-NIR upconversion: Figure 2 shows the energy level diagram and relevant optical processes for the Yb^{3+}/Tm^{3+} doped upconversion system. The Yb^{3+} ion acts as a sensitizer and the

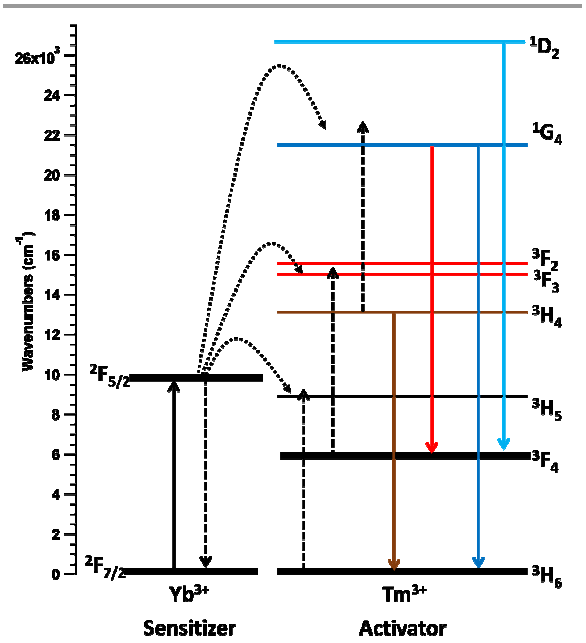

Figure 2: Schematic representation of NIR-to-Visible and NIR-to-NIR upconversion in Yb^{3+}/Tm^{3+} doped β-$NaYF_4$ UCNPs excited with 980 nm light. Sequential energy transfers from the Yb^{3+} ions (sensitizer) to the Tm^{3+} ions (activator) populate successively higher energy states of Tm^{3+} resulting in NIR (800 nm), red (650 nm) and blue (450 nm, 475 nm) upconversion emission.

Tm^{3+} ion acts as an activator, producing visible and NIR emission. The Yb^{3+} sensitizers absorb 980 nm excitation light and transfers energy to adjacent Tm^{3+} activator ions. Multiple sequential $Yb^{3+} \rightarrow Tm^{3+}$ energy transfer events promote the

Tm^{3+} ions to successively higher energy levels. There is some doubt as to how the $^1D_2$ state of Tm^{3+} is populated, so that this excitation pathway is not labelled in Figure 2. (It has been suggested that the final step to populate $^1D_2$ requires $Tm^{3+} \rightarrow Tm^{3+}$ energy transfer.)[45, 46] Blue emission is observed from the $^1D_2$ and $^1G_4$ excited states of Tm^{3+} ion, corresponding to the $^1D_2 \rightarrow {}^3F_4$ (450 nm) and $^1G_4 \rightarrow {}^3H_6$ (475 nm) transitions. NIR emission is observed from the $^3H_4$ and $^1G_4$ emitting levels, corresponding to the $^3H_4 \rightarrow {}^3H_6$ (800 nm) and $^1G_4 \rightarrow {}^3H_5$ (780 nm) transition, the latter of which is not labelled in Figure 2. Weak red emission is also observed, corresponding to the $^1G_4 \rightarrow {}^3F_4$ (650 nm) transition.

Yb^{3+}/Tm^{3+}-doped β-$NaYF_4$ nanoparticles have been studied primarily relative to their NIR-to-blue upconversion properties, with the doping levels chosen to optimize the blue upconversion emission. This blue emission is excited via three- and four-photon processes, whereas the NIR-to-NIR $^3H_4 \rightarrow {}^3H_6$ emission at 800 nm is excited via a two-photon process. As a result, the 800 nm NIR-to-NIR emission is much more intense than the NIR-to-blue emission, particularly at modest excitation power densities, P_{exc}. For example, even for β-$NaYF_4$: 25%Yb^{3+}/0.3%Tm^{3+}, which is optimized for blue emission, NIR emission is 400× more intense than blue emission at P_{exc}=6.2 W/cm^2 and 100× more intense at P_{exc}=35 W/cm^2. (See Figure 3).

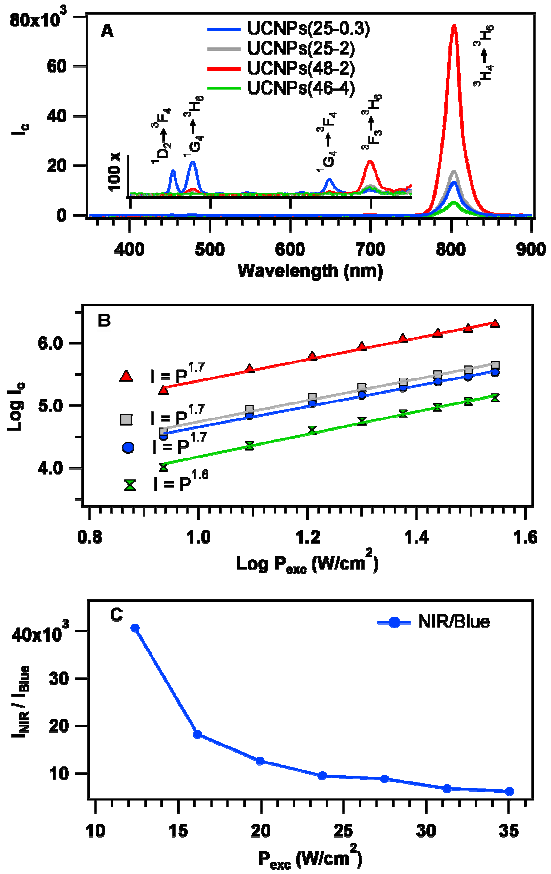

Figure 3: A) Comparison of upconversion emission, I_c, spectra of β-$NaYF_4$ nanoparticles with various Yb^{3+}/Tm^{3+} doping levels dispersed in toluene. Excitation was at 980 nm (35 W/cm^2). The spectra represent a valid comparison of relative brightness of samples (in terms of number photons emitted per constant wavelength interval) corrected to equal number densities of nanoparticles (See Equation 1). The insert shows a 100× magnification of the visible region of the spectra. **B)** Log-log plot of the dependence of the 800 nm NIR emission intensity on excitation power density, P_{exc}. **C)** NIR-to-blue emission intensity ratio, I_{NIR}/I_{Blue} for UCNPs(48-2) as a function of excitation power density, P_{exc}.

For the initial phase of this study, we determine the optimum doping levels for maximizing the absolute brightness of 800 nm emission, with the secondary purpose of minimizing the blue emission. The absolute brightness of the 800 nm emission determines the minimum P_{exc} required to view the NIR-to-NIR upconversion images shown later in this article. For print applications for which no opaque coatings are applied, minimizing the blue emission is necessary in order to maintain the covert nature of the images. When using opaque coatings, only the absolute brightness of 800 nm emission is of interest.

We synthesized UCNPs with four doping combinations of Yb^{3+} and Tm^{3+}: 25%Yb^{3+}/0.3%Tm^{3+} (UCNPs(25-0.3)), 25%Yb^{3+}/ 2%Tm^{3+} (UCNPs(25-2)), 48%Yb^{3+}/2%Tm^{3+} (UCNPs (48-2)), and 46%Yb/4%Tm^{3+} (UCNPs(46-4)). The emission spectra were recorded by exciting the UCNPs with a 980 nm CW laser using a range of excitation power densities, P_{exc}=5-35 W/cm^2. Figure 3A compares the UC emission spectra of the four compounds dispersed in toluene using P_{exc}=35 W/cm^2. The insert shows the NIR-to-Visible portion of the spectrum magnified by 100×. Clearly, even at the highest P_{exc} values used, the spectra are completely dominated by the 800 nm emission.

The peak assignments in Figure 3A are largely consistent with those reported in the literature.[4, 46] The NIR emission is dominated by the $^3H_4 \rightarrow {}^3H_6$ transition at 800 nm, which is excited via a two-photon process. At higher excitation power densities (not used here), a significant NIR contribution at 780 nm from the $^1G_4 \rightarrow {}^3H_5$ transition, excited via a three-photon process, becomes evident, usually appearing as a strong shoulder to the 800 nm peak.[47] The blue peaks at 450 nm and 475 nm correspond to the $^1D_2 \rightarrow {}^3F_4$ and $^1G_4 \rightarrow {}^3H_6$ transitions, excited via four- and three-photon processes, respectively.

There has been some confusion regarding the origin of the red emission at 650 nm, which has been variously assigned in the literature as arising from $^3F_{3,2}$ or from $^1G_4$. Yan *et al.* report that the 475 nm and 650 nm emission intensity exhibit similar dependence on excitation power, consistent with both transitions arising from $^1G_4$.[48] Moreover, we observe that the relative intensities of 475 nm and 650 nm emission remain constant at all doping concentrations, indicating that these transitions experience the same quenching effects, and, therefore, originate from the same emitting state. Finally, we also observe that the time profiles of 475 nm and 650 nm emission following pulsed 980 nm excitation are nearly identical, strongly supporting the assignment of the 650 nm emission arising from the $^1G_4$ state. Therefore, the 650 nm

emission is assigned as being predominately due to the $^1G_4 \rightarrow {}^3F_4$ transition.

The emission at 700 nm is tentatively assigned to $^3F_{3,2} \rightarrow {}^3H_6$ based on the fact that this is the expected wavelength for this emission, and on the fact that this peak shows a power dependence similar to that of the 800 nm emission, $^3H_4 \rightarrow {}^3H_6$ (See Supporting Information). Referring to Figure 2, emission from $^3F_{3,2}$ and $^3H_4$ are expected to have similar power dependence, because $^3H_4$ is fed through the $^3F_{3,2}$ states. We note, however, that the 700 nm peak is observed in some spectra reported in the literature, but not in others. The reason for this is unclear to us. We note, however, that the relative intensity of the 700 nm transition will be very sensitive to multi-phonon quenching because the $^3F_{3,2}$-$^3H_4$ energy gap is so small. This emission may then vary somewhat from sample to sample due to otherwise minor differences in sample properties.

The spectra in Figure 3A represent the relative brightness of the different sample dispersions corrected to equal number densities of nanoparticles. Corrected spectra, I_C, were generated from the measured spectra, I_M, using the following formula:

$$I_C = I_M \times \%Yb \,/\, A(980\ nm) \qquad (1)$$

where, %Yb is the doping concentration in the nanocrystals and A(980 nm) is the sample absorbance at 980 nm. A quantitative comparison of the relative brightness of the blue, I_C(Blue), and NIR, I_C(NIR), upconversion for the different doping combinations represented in Figure 3A is summarized below in Table 1. The 48%Yb^{3+}/2%Tm^{3+} sample yields both the brightest 800 nm emission and the highest NIR/blue emission ratio. We note that this optimal doping combination holds for the modest excitation power densities ($P_{exc} \leq 35$ W/cm^2) used in our imaging process. Zhao *et al*. have shown that the optimal concentration for a given emission wavelength can be different at high excitation power densities.[29]

Table 1. Relative brightness of the blue and NIR upconversion for different sample dispersions corrected to equal number densities of nanoparticles. Corrected intensities, I_C, were generated from the measured spectra, I_M, using Eq. 1.

%Yb	%Tm	I_c (NIR)	I_c(Blue)x10^2	I_cNIR/I_cBlue
25	0.3	1.0	0.97	103
25	2	1.3	0.03	4366
48	2	5.8	0.09	6207
46	4	0.4	0.01	3146

Referring to Figure 3A, several important trends are evident. First, blue emission is increasingly quenched with increasing Tm concentration, whereas the NIR (800 nm) emission initially increases marginally, and then drops precipitously. These observations are consistent with a previous study by Quintanilla *et al*.[46] that reported strong Tm concentration quenching of both $^1D_2$ and $^1G_4$ with a more modest effect on emission from $^3F_{2,3}$ and $^3H_4$. Similarly, Zhao *et al*. also reported a decrease in 800 nm emission with increasing Tm concentration in 20% Yb^{3+}/0.2-4%Tm^{3+} doped β-$NaYF_4$ crystals at 10 W/cm^2 excitation power density.[29] Thus, the optimal Tm concentration for our purposes, quenching blue emission while having little or no detrimental effect on 800 nm emission, can be identified as being quite close to the 2% level. With regard to %Yb concentration, over the range of excitation power densities used here, the corrected intensity, I_C, of 800 nm emission continues to increase as Yb concentration is raised beyond 25%. However, we limit the Yb doping to 48% because it becomes increasingly difficult to control the size and phase stability of the nanocrystals at higher doping levels, as discussed by Damasco, et. al, and references therein.[49]

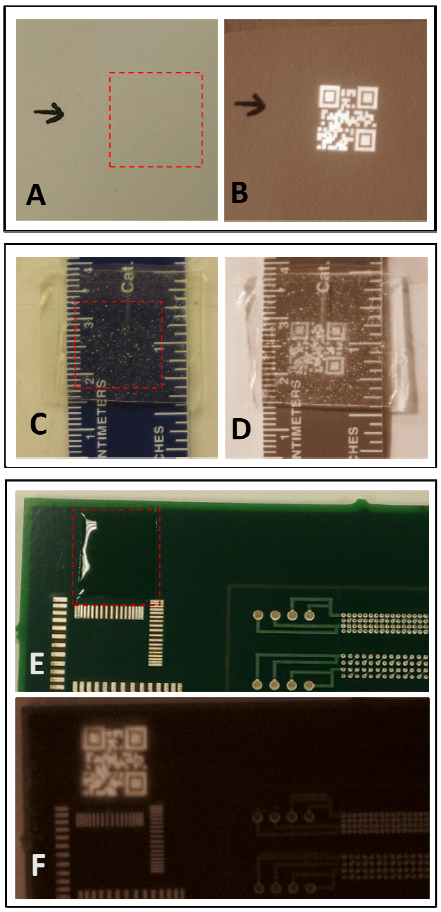

Figure 4: Ambient light photographs of covert QR codes printed with NIR-to-NIR upconversion ink activated with NIR-optimized nanoparticles (UCNPs(48-2)) on a (A) plain paper; (C) laminated between transparent epoxy films; and (E) on an electronic circuit board and subsequently coated with a protective layer of transparent epoxy. The printed patterns are invisible under ambient conditions. The NIR luminescent images (800 nm) of QR codes in A, C, and E images can be easily captured, corresponding to B, D, and F, respectively, with a NIR sensitive camera using 980 nm illumination (P_{exc}= 1.5 W/cm^2).

Figure 3C shows the ratio of 800 nm-to-blue emission for UCNPs(48-2) as a function of P_{exc} over the range of excitation power densities used in this study. Even at the highest P_{exc} values, 800 nm emission is >6000× more intense than the blue emission. As noted below, 800 nm luminescent images can be read easily with a modified point-and-shoot camera using laser power densities at which little or no visible emission is detectable by eye.

NIR-to-NIR imaging of printed patterns: The NIR-optimized UCNPs(48-2) were formulated into inks and used to print 1 cm x 1 cm QR codes on a variety of substrates. Figure 4 shows photographs of these QR codes, under ambient lighting and 980-nm excitation, printed on plain paper (Figures 4A,B), laminated between transparent epoxy films (Figures 4C,D), and printed on an electronic circuit board (Figures 4E,F).

The locations of the printed areas in the ambient-lighting photographs are indicated by a red dotted box. In all cases, the printed QR codes are invisible to the naked eye under ambient light. The images of the QR codes under ambient light were captured with smart-phone camera (Figures 4A, 4C and 4E), whereas the 800 nm luminescent images generated by 980-nm excitation (Figures 4B, 4D and 4F) were captured with a point-and-shoot camera, modified as described above. At the excitation power densities used to acquire the luminescent images shown in Figure 4 (P_{exc} =1.5 W/cm^2), blue emission is either undetectable or very faint.

The QR code printed on a plain paper (Figure 4A) generates a very bright, sharp 800 nm luminescent image (Figure 4B) even under relatively low excitation flux (P_{exc}= 1.5 W/cm^2).

Figure 4C shows an ambient-light photograph of sample prepared by printing a QR code on a 0.2 mm thick transparent epoxy layer followed by coating with another 0.2 mm thick transparent epoxy layer. The laminated sample was placed on a ruler to assist the reader in judging its size and optical quality. The NIR luminescent image of the QR code was captured with the NIR sensitive camera using 980 nm excitation P_{exc}= 1.5 W/cm^2 (Figure 4D). The image is not as bright or sharp as that of the QR code on paper due to the imperfect optical quality of the epoxy matrix, caused in part by air bubbles entrapped in the epoxy film while mixing the hardener and resin, and by lensing effects arising from the topography of the epoxy surface.

Figure 4E is a photograph of the upconversion ink printed on an electronic circuit board and then coated with a protective thin film (0.4 mm) of transparent epoxy. The QR code retained its integrity after coating with the epoxy. A distinct NIR luminescent image of QR code was captured by exciting the printed region with 980 nm light, P_{exc}= 1.5 W/cm^2 (Figure 4F). The epoxy film has high degree of transparency and does not significantly attenuate the transmission of excitation (980 nm) or emission (800 nm) light. The experiment demonstrates the ability to protect the security feature with durable coatings without adversely affecting functionality.

Imaging printed features through opaque coatings: Because the imaging proposed herein utilizes emission and excitation in the NIR, it is possible to coat and protect these images with materials that are visibly opaque. This strategy strengthens the covert nature of the print / read system and offers some additional advantages over bare prints or transparent-layer protective coatings. First, even if otherwise viewable intensities of visible emission are generated by the NIR excitation, the opaque coating will block these wavelengths. Second, the invisibility of the latent print image on the uncoated substrate is no longer a requirement. This permits the use of higher particle loadings or thicker print coatings, which, in turn, lower the threshold of P_{exc} required to view and capture the image.

We use two methods to apply opaque coatings to the UC printed features. Both methods use opaque coatings based on commercially available, water-based inkjet-printer ink from Hobbicolor (Black). The transmission spectrum of the ink (20 µL of ink in 5 mL of water) measured across 1 cm path length has <1% transmission in the visible region and >95% transmission in the NIR region. (See Figure 5). Also, for this set of experiments, we use inks activated with the UCNPs(25-0.3) taggants, optimized for blue emission, in order to judge the ability of the opaque coatings to block visible emission from the printed images.

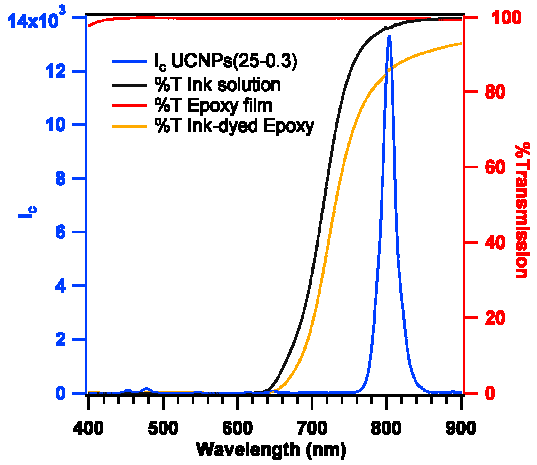

Figure 5: (Blue) Upconversion emission, I_c, spectrum of 1 wt% UCNPs (25-0.3) in toluene excited with 980 nm laser. Transmission spectra of (Black) black inkjet ink solution (20 µL of Hobbicolors ink in 5 mL of water, 1 cm path length); (Red) 0.4 mm thick epoxy film and; (Orange) 0.4 mm thick epoxy film dyed with black inkjet ink.

In the first method, an inkjet printer loaded with the Hobbicolor Black cartridge is used to print over UC print features that were previously applied to the paper. In the second method, a UC print feature is coated with a layer of black epoxy (dyed with 0.03 mL of Hobbicolor ink per 1 mL epoxy). The transmission spectra of a 0.4 mm thick epoxy layer before and after dying with black ink are shown in Figure 5. The undyed epoxy film has a high degree of transmittance in the visible as well as NIR region. The black epoxy film has <1% transmittance in the visible region, but retains >80% transmittance in the relevant NIR region.

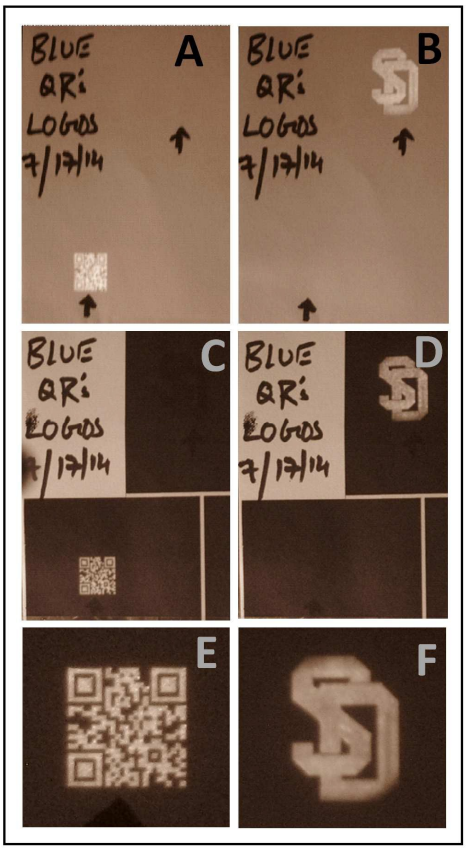

Figure 6: NIR upconversion images from patterns printed on paper using inks activated with UCNPs(25-0.3). Images were captured with a NIR sensitive camera exciting with 980 nm light (P_{exc}= 1.5 W/cm^2). The printed patterns are invisible to the naked eye under ambient conditions, but emit blue and 800 nm light upon excitation with NIR laser. Images A and B correspond to images acquired prior to application of a black inkjet overcoating. Images C and D correspond to A and B, respectively, after application of the black inkjet overcoating. Images E and F are magnified sections of the luminescent patterns shown in C and D, respectively.

Figures 6A and 6B are images of the UCNPs(25-0.3) printed on a plain paper, acquired with a NIR-sensitive camera under ambient lighting. The black arrows indicate the positions of the printed features. The lower-left printed image in Figure 6A is being illuminated with 980 nm laser excitation, and the UC luminescent image of the QR code is clearly visible. Similarly, the UC luminescent image of University of South Dakota logo was captured in Figure 6B. For Figures 6A and 6B, it is possible to detect very faint blue emission with the naked eye. (Blue emission becomes visible when excitation power densities in the range of P_{exc}= 4.0-5.5 W/cm^2 are used.)[20, 21] This blue emission is not evident in the camera images of Figures 6A and 6B, because it is overwhelmed by the intensity of the 800 nm emission. Figures 6C and 6D show images corresponding to Figures 6A and 6B after the same sheet of paper was passed through an inkjet printer and coated with black ink. The NIR images can be easily captured through the printed coatings with no significant attenuation relative to those obtained prior to coating. The faint blue emission is now, however, completely blocked and no trace of the images are evident to the naked eye, even upon increasing excitation power densities to levels normally used to view blue upconversion (P_{exc}= 5 W/cm^2). Figures 6E and 6F are magnified images (5×) of the luminescent images shown in the Figure 6C and 6D, respectively. The images retain good detail even after coating with black inkjet ink.

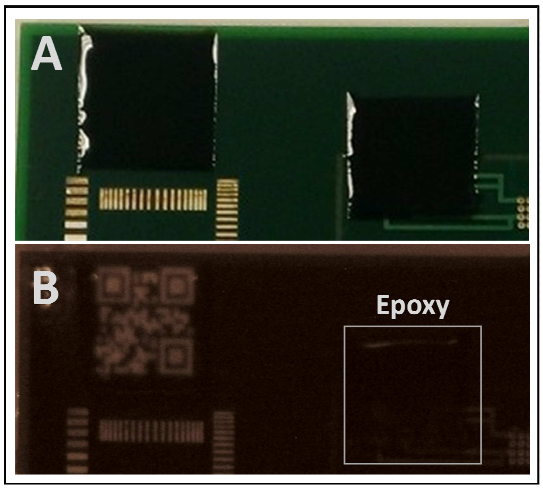

Figure 7: (A) Upconversion QR code printed on an electronic circuit board with blue (UCNPs(25-0.3)) upconversion ink and subsequently coated with a secondary protective layer of opaque, black epoxy. (B) Under 980 nm excitation (1.5 W/cm^2), the black epoxy blocks the visible upconversion, but transmits the NIR light. The 800 nm luminescent image was captured with a NIR sensitive camera.

In the second method, we use a dyed epoxy resin as the opaque protective coating. A 1 cm x 1 cm QR code was printed with blue-optimized upconversion ink on an electronic circuit board. This print was then coated with a 0.4 mm layer of black-ink-doped epoxy overcoat. The transmittance spectrum of this layer is shown in Figure 5. Figure 7A shows an ambient-lighting photograph of the epoxy-coated electronic circuit taken with a smartphone. The UCNPs printed region was excited with a 980 nm laser (P_{exc}= 1.5 W/cm^2) through the black epoxy layer. Although the printed features are not visible to the naked eye, they are easily captured using a NIR sensitive camera (Figure 7B). The blue emission, however, was completely blocked by the black epoxy coating, even at P_{exc}= 5 W/cm^2. The highlighted box in Figure 7B shows another QR code coated with the black epoxy, which was not excited with 980 nm light, and, therefore, shows no NIR emission.

We note that the luminescent images shown in Figs. 6 and 7 are not as bright as those shown in Figure 4, due to the fact that blue-optimized nanoparticles (UCNPs(25-0.3)) were used to formulate the inks for these samples in order to test the efficacy of the opaque coatings in blocking any visible blue emission.

Figure 8 shows examples of covert images printed using NIR-optimized inks (UCNPs(48-2)) on a circuit board. The images on the left are coated with black epoxy, whereas the images on the right are coated with transparent epoxy. Bright,

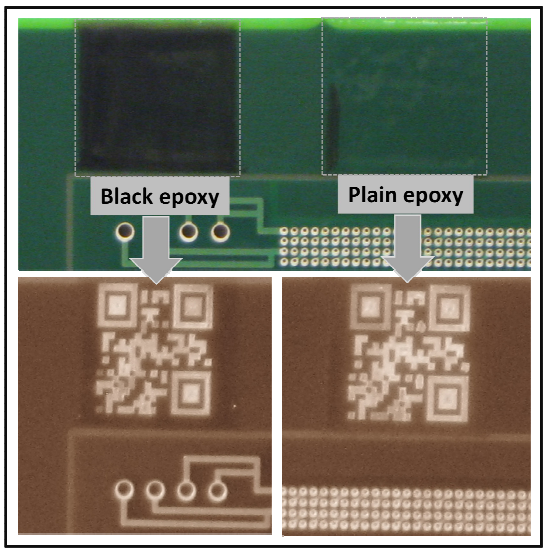

Figure 8: (Top) QR codes (1 cm x 1 cm) printed on an electronic circuit with NIR-to-NIR upconversion ink activated with NIR-optimized UCNPs(48-2) and coated with black (upper left) and transparent (upper right) epoxy. (Bottom) Upon 980 nm illumination, the NIR luminescent images are clearly visualized using a modified point-and-shoot camera. The brightness of the image read through the black epoxy (lower left) is comparable to that read through the transparent epoxy. The QR codes show retention of integrity after epoxy coating.

distinct, NIR luminescent images from both print areas, produced with modest 980 nm excitation density (P_{exc}= 1.5 W/cm^2), are easily captured with our modified point-and-shoot camera. The epoxy coatings do not adversely affect the integrity of the printed images. Moreover, the image acquired through the black epoxy coating is nearly as bright as that acquired through the transparent epoxy.

Conclusion

The print-and-read security printing system described herein, based on NIR-to-NIR inks, offers a high level of covertness and can be made tamper-evident when combined with hard, opaque coatings. The inks are activated with Yb^{3+}/Tm^{3+} doped β-$NaYF_4$ UCNPs, and it is determined that the optimal doping levels for maximizing the brightness of 800-nm upconversion and minimizing the undesired blue upconversion is 48%Yb^{3+}/2%Tm^{3+}. For the NIR-optimized UCNPs, the NIR-to-NIR intensity is greater than 6000× that of the NIR-to-blue emission, even at relatively high excitation power densities (35 W/cm^2). The upconversion images, generated with 980-nm excitation, cannot be seen with the naked eye, but are easily captured with an inexpensive, modified point-and-shoot digital camera. The 800 nm upconversion emission is near perfect for detection with a digital camera, since this wavelength is at or near the peak sensitivity of the CCD chip. All images tested are easily captured with a modified point-and-shoot camera using modest excitation power densities (1.5 W/cm^2).

Electronic circuit boards, plain paper, and epoxy-resin films are shown to be suitable substrates to demonstrate the application. Inkjet printing or epoxy coatings applied over the upconversion prints do not erode the print integrity. It is demonstrated that the NIR-to-NIR images can be read through opaque coatings of inkjet printing or black epoxy resin, with no significant loss of brightness. The use of durable opaque coatings offers a significant advantage to the covert print system for three reasons: (1) it deters tampering; (2) it increases the covert nature of the marking, both in terms of the latent image, and in terms of the luminescent image (by blocking visible emission); and (3) it relaxes the requirement that the bare printed image be completely covert.

The ability to read the covert code or symbol across an opaque protective layer makes the current system attractive for numerous security and anti-counterfeiting applications, including electronic circuit boards and high-value integrated circuits.

Acknowledgment

The authors acknowledge generous support from NSF (EPS-0903804, DGE-0903685, CHE-0840507, IIP 1414211). C. Douma and D. Langerman were supported by an NSF:REU award to Crawford and May (EEC 1263393). P.S.M. acknowledges support from NASA (Cooperative Agreement Number: NNX10AN34A). Additional support was provided through a Collaboration grant to J. Kellar from the State of South Dakota, Governor's Office of Economic Development.

Abbreviations

UCNPs, Upconversion nanoparticles;

UCNPs(25-0.3), 25%Yb^{3+}/0.3%Tm^{3+} doped β-$NaYF_4$ UCNPs;

UCNPs(25-2), 25%Yb^{3+}/2%Tm^{3+} doped β-$NaYF_4$ UCNPs;

UCNPs(48-2), 48%Yb^{3+}/2%Tm^{3+} doped β-$NaYF_4$ UCNPs;

UCNPs(46-4), 46%Yb^{3+}/4%Tm^{3+} doped β-$NaYF_4$ UCNPs.

References

1. E. M. Chan, D. J. Gargas, P. J. Schuck and D. J. Milliron, *The Journal of Physical Chemistry B*, 2012, **116**, 10561-10570.
2. Q. Meng, R. J. Witte, Y. Gong, E. L. Day, J. Chen, P. S. May and M. T. Berry, *Chem. Mater.*, 2010, **22**, 6056-6064.
3. F. Wang, D. Banerjee, Y. Liu, X. Chen and X. Liu, *Analyst*, 2010, **135**, 1839-1854.
4. S. Heer, K. Kömpe, H. U. Güdel and M. Haase, *Advanced Materials*, 2004, **16**, 2102-2105.
5. F. Vetrone and J. A. Capobianco, *International Journal of Nanotechnology*, 2008, **5**, 1306-1339.
6. M. Haase and H. Schäfer, *Angewandte Chemie International Edition*, 2011, **50**, 5808-5829.
7. F. Wang and X. Liu, *Chemical Society Reviews*, 2009, **38**, 976-989.
8. C. Hazra, V. N. K. B. Adusumalli and V. Mahalingam, *ACS Applied Materials & Interfaces*, 2014, **6**, 7833-7839.

9. L. Zhao, J. Peng, M. Chen, Y. Liu, L. Yao, W. Feng and F. Li, *ACS Applied Materials & Interfaces*, 2014, **6**, 11190-11197.
10. G. Chen, H. Qiu, P. N. Prasad and X. Chen, *Chemical Reviews*, 2014, **114**, 5161-5214.
11. Y. Ma, S. Huang, M. Deng and L. Wang, *ACS Applied Materials & Interfaces*, 2014, **6**, 7790-7796.
12. S. Liu, L. Zhang, T. Yang, H. Yang, K. Y. Zhang, X. Zhao, W. Lv, Q. Yu, X. Zhang, Q. Zhao, X. Liu and W. Huang, *ACS Applied Materials & Interfaces*, 2014, **6**, 11013-11017.
13. Q. Liu, J. Peng, L. Sun and F. Li, *ACS Nano*, 2011, **5**, 8040-8048.
14. L. Zhou, B. He, J. Huang, Z. Cheng, X. Xu and C. Wei, *ACS Applied Materials & Interfaces*, 2014, **6**, 7719-7727.
15. Q. Zhan, J. Qian, H. Liang, G. Somesfalean, D. Wang, S. He, Z. Zhang and S. Andersson-Engels, *ACS Nano*, 2011, **5**, 3744-3757.
16. Y.-F. Wang, G.-Y. Liu, L.-D. Sun, J.-W. Xiao, J.-C. Zhou and C.-H. Yan, *ACS Nano*, 2013, **7**, 7200-7206.
17. G. Chen, J. Shen, T. Y. Ohulchanskyy, N. J. Patel, A. Kutikov, Z. Li, J. Song, R. K. Pandey, H. Ågren, P. N. Prasad and G. Han, *ACS Nano*, 2012, **6**, 8280-8287.
18. Z. Hou, X. Li, C. Li, Y. Dai, P. a. Ma, X. Zhang, X. Kang, Z. Cheng and J. Lin, *Langmuir*, 2013, **29**, 9473-9482.
19. L. He, L. Feng, L. Cheng, Y. Liu, Z. Li, R. Peng, Y. Li, L. Guo and Z. Liu, *ACS Applied Materials & Interfaces*, 2013, **5**, 10381-10388.
20. J. M. Meruga, A. Baride, W. Cross, J. J. Kellar and P. S. May, *Journal of Materials Chemistry C*, 2014, **2**, 2221-2227.
21. J. M. Meruga, W. M. Cross, P. S. May, Q. Luu, G. A. Crawford and J. J. Kellar, *Nanotechnology*, 2012, **23**, 395201.
22. T. Blumenthal, J. Meruga, P. S. May, J. Kellar, W. Cross, K. Ankireddy, S. Vunnam and Q. N. Luu, *Nanotechnology*, 2012, **23**, 185305.
23. N. M. Sangeetha, P. Moutet, D. Lagarde, G. Sallen, B. Urbaszek, X. Marie, G. Viau and L. Ressier, *Nanoscale*, 2013, **5**, 9587-9592.
24. M.-K. Tsang, G. Bai and J. Hao, *Chemical Society Reviews*, 2015, DOI: 10.1039/C4CS00171K.
25. J. Lee, P. W. Bisso, R. L. Srinivas, J. J. Kim, A. J. Swiston and P. S. Doyle, *Nat Mater*, 2014, **13**, 524-529.
26. Y. Zhang, L. Zhang, R. Deng, J. Tian, Y. Zong, D. Jin and X. Liu, *Journal of the American Chemical Society*, 2014, **136**, 4893-4896.
27. B. Yoon, J. Lee, I. S. Park, S. Jeon, J. Lee and J.-M. Kim, *Journal of Materials Chemistry C*, 2013, **1**, 2388-2403.
28. W. J. Kim, M. Nyk and P. N. Prasad, *Nanotechnology*, 2009, **20**, 185301.
29. J. Zhao, D. Jin, E. P. Schartner, Y. Lu, Y. Liu, A. V. Zvyagin, L. Zhang, J. M. Dawes, P. Xi, J. A. Piper, E. M. Goldys and T. M. Monro, *Nat Nano*, 2013, **8**, 729-734.
30. J.-C. Boyer, F. Vetrone, L. A. Cuccia and J. A. Capobianco, *Journal of the American Chemical Society*, 2006, **128**, 7444-7445.
31. J.-C. Boyer, L. A. Cuccia and J. A. Capobianco, *Nano Letters*, 2007, **7**, 847-852.
32. F. Auzel and D. Pecile, *Journal of Luminescence*, 1976, **11**, 321-330.
33. S. Gai, C. Li, P. Yang and J. Lin, *Chemical Reviews*, 2014, **114**, 2343-2389.
34. R. Lv, G. Yang, F. He, Y. Dai, S. Gai and P. Yang, *Nanoscale*, 2014, **6**, 14799-14809.
35. R. Lv, C. Zhong, R. Li, P. Yang, F. He, S. Gai, Z. Hou, G. Yang and J. Lin, *Chemistry of Materials*, 2015, **27**, 1751-1763.
36. R. H. Page, K. I. Schaffers, P. A. Waide, J. B. Tassano, S. A. Payne, W. F. Krupke and W. K. Bischel, *J. Opt. Soc. Am. B*, 1998, **15**, 996-1008.
37. L. Zhengquan and Z. Yong, *Nanotechnology*, 2008, **19**, 345606.
38. J. Zhang, H. Zhao, X. Zhang, X. Wang, H. Gao, Z. Zhang and W. Cao, *The Journal of Physical Chemistry C*, 2014, **118**, 2820-2825.
39. F. Wang and X. Liu, *Journal of the American Chemical Society*, 2008, **130**, 5642-5643.
40. Q. Liu, Y. Sun, T. Yang, W. Feng, C. Li and F. Li, *Journal of the American Chemical Society*, 2011, **133**, 17122-17125.
41. J.-C. Boyer, M.-P. Manseau, J. I. Murray and F. C. J. M. van Veggel, *Langmuir*, 2009, **26**, 1157-1164.
42. N.-N. Dong, M. Pedroni, F. Piccinelli, G. Conti, A. Sbarbati, J. E. Ramírez-Hernández, L. M. Maestro, M. C. Iglesias-de la Cruz, F. Sanz-Rodriguez, A. Juarranz, F. Chen, F. Vetrone, J. A. Capobianco, J. G. Solé, M. Bettinelli, D. Jaque and A. Speghini, *ACS Nano*, 2011, **5**, 8665-8671.
43. M. Nyk, R. Kumar, T. Y. Ohulchanskyy, E. J. Bergey and P. N. Prasad, *Nano Letters*, 2008, **8**, 3834-3838.
44. C. Lin, M. T. Berry, R. Anderson, S. Smith and P. S. May, *Chemistry of Materials*, 2009, **21**, 3406-3413.
45. T. Riedener, H. U. Güdel, G. C. Valley and R. A. McFarlane, *Journal of Luminescence*, 1995, **63**, 327-337.
46. M. Quintanilla, N. O. Nunez, E. Cantelar, M. Ocana and F. Cusso, *Nanoscale*, 2011, **3**, 1046-1052.
47. Q. Luu, A. Hor, J. Fisher, R. B. Anderson, S. Liu, T.-S. Luk, H. P. Paudel, M. Farrokh Baroughi, P. S. May and S. Smith, *The Journal of Physical Chemistry C*, 2014, **118**, 3251-3257.
48. A. Yin, Y. Zhang, L. Sun and C. Yan, *Nanoscale*, 2010, **2**, 953-959.
49. J. A. Damasco, G. Chen, W. Shao, H. Ågren, H. Huang, W. Song, J. F. Lovell and P. N. Prasad, *ACS Applied Materials & Interfaces*, 2014, **6**, 13884-13893.

Table of Contents Graphic